13th World Conference on Earthquake Engineering
Vancouver, B.C., Canada
August 1-6, 2004
Paper No. 2929

MODELLING OF A PARTIAL-STRENGTH BEAM-TO-COLUMN JOINT FOR HIGH DUCTILE STEEL-CONCRETE COMPOSITE MR FRAMES

W. SALVATORE[1], A. BRACONI[2], O. S. BURSI[3], and R. TREMBLAY[4]

SUMMARY

The paper describes the behaviour and component modelling of partial strength beam-to-column joints used in high ductile steel-concrete composite moment-resisting frame structures. The joint performance was determined via quasi-cyclic and monotonic tests conducted on subassemblages at the University of Pisa and a series of pseudo-dynamic tests executed on a full-scale two-storey frame structure specimen at the European Laboratory for Structural Assessment (ELSA) of the Joint Research Centre (JRC). The joints analysed are composed of extended end-plate connections whose inelastic response is divided mainly between shear yielding of the column web panel and inelastic bending of the extended end plate and column flange. Also yielding of the slab reinforcements and concrete crushing against the face of the columns took place during testing. Analytical models of internal joints were developed on the basis of experimental results and formulae on subassemblages. In detail, experimental laws governing the response of joint components were obtained by using only equilibrium and kinematic considerations to process experimental data. Results obtained permitted existing laws to be validated, some of which with current European standards.

INTRODUCTION

The capacity design criterion can be used to ensure that traditional structures can reach high energy dissipation levels without significant strength reduction in order to exhibit good performance under seismic ground motions. In general, high-ductility structures must withstand low seismic actions having short return periods without undergoing appreciable damage. For high-intensity earthquakes, structures must exploit their plastic resources to dissipate seismic energy, thereby sustaining substantial damage, while maintaining overall structural stability. Solutions to achieve the necessary ductility can be obtained through careful study of building morphology, structural schemes and construction details, but also through the rational use of materials. In this perspective, steel-concrete structures appear to be the most convenient both for constructional and for economic aspects. When analyzing possible structural solutions, it becomes evident that the use of composite beams and columns that exhibit superior stiffness

[1] *Assistant Professor, University of Pisa, Italy, walter@ing.unipi.it*
[2] *PhD student, University of Pisa, Italy, a.braconi@ing.unipi.it*
[3] *Full Professor, Dept. of Mech. and Struct. Eng., University of Trento, Italy, oreste.bursi@ing.unitn.it*
[4] *Full Professor, Ecole Polytechnique, Montreal, Canada, tremblay@struc.polymtl.ca*

properties can limit significantly second-order effects and allow buildings of considerable height without any additional bracing to be erected. This advantage, combined to the use of partial strength joints, guarantees the formation of global dissipative frame mechanisms for seismic loads, while avoiding undesirable storey or local mechanisms. If associated to suitable constructional solutions, such structural schemes can undoubtedly provide significant advantages in terms of both economy and performance [1]. However, to date, the adoption of steel-concrete composite structures in design practice has been precluded by the lack of suitable construction solutions. A new solution has been recently proposed within the framework of two European research projects, ECSC 7210-PR-250 [2] and ECOLEADER HPR-CT-1999-00059 [3], which have permitted the efficiency of moment resisting (MR) frame structures with partial strength joints to be verified [4]. The application of current European rules to this case study has revealed their inadequacies in terms of seismic design of high ductile composite beam-to-column joints. The rules do not propose component models for seismic loading capable of adequately simulating joint behaviour in terms of strength, stiffness and rotational capacity for either sagging or hogging bending moments [5-7]. In detail, mechanisms by which the forces are transmitted between the reinforced concrete slab and composite columns have yet to be clarified. In the case of internal beam-to-column joints, the behaviour is governed by interaction phenomena between forces transmitted by the two beams framing into the joint. Moreover, capacity design criteria for components are not provided. A similar situation can be found in U.S. [8] where research is still ongoing [9].

This paper presents a description and an analysis of test results performed at the Materials Testing Laboratory of the University of Pisa within the framework of an ECSC research project [2]. A series of experimental measurements were obtained on subassemblages representative of internal beam-column joints. Using this data and analytical formulae, it was possible to define joint response laws, as well as those of individual structural elements and components of an accurate mechanical model specifically developed to characterize such joints. Some experimental laws for components of the proposed mechanical model are then compared to analytical models and standards in order to verify their accuracy.

SEISMIC DESIGN OF A COMPOSITE BEAM-TO-COLUMN JOINT

The proposed structural solution consists of composite beams made of hot-rolled steel profiles connected with studs to a 150 mm-thick concrete slab cast on a collaborating ribbed steel sheet, as illustrated in Fig. 1. Full shear connection is provided between the steel profile and the concrete slab. The columns are made of partially encased hot-rolled steel profiles, which ensures significant structural efficiency for both static and seismic loads, as well as good fire resistance. The solution, depicted in Fig 2, also offers the advantage of not requiring any welding between the reinforcing bars. However, the reinforced concrete fill must be properly secured to the steel profile by means of steel studs to develop effective collaboration and avoid detachment of the concrete. The beam-to-column joint has been designed to provide adequate structural performance under both monotonic and cyclic loading. To this aim, a relatively thin end-plate connection (Fig. 3) has been chosen because of its efficiency and predictable performance under seismic demand. The reinforced concrete encasement is interrupted at the joint level, as shown in Figs. 3 and 4, and the column is left in the bare steel condition for constructional considerations and suitable seismic behaviour of the column web panel [1]. A pair of horizontal stiffening plates welded to the column permits full exploitation of the web panel inelastic resources. The stirrups, external to the central area of the joint, are arranged within the critical length, as per the provisions of Eurocode 8 [7] (see Fig. 3).

The ductile behaviour of the joints is achieved by defining an appropriate hierarchy of resistance for all the components. In this respect, with reference to sagging moments, the end-plate and column flange responding in bending, as well as the column web panel acting in shear are all to be considered as ductile components; whereas the concrete slab under compression and the bolts under tension are assumed to be brittle. With regard to hogging moments, the steel reinforcing bar in tension, the end-plate and the column

flange acting bending, and the column web panel under shear are considered ductile components; while the column web panel and the beam flanges resisting compression are assumed to be brittle [10]. The joint also had to possess adequate resistance and rotational capacity [11]. Capacity design of the partial strength joints was performed by taking into account the variability of the material properties. The final joint details are reported in Table 1. As a result, introducing the actual material properties did not modify the location of the yield regions.

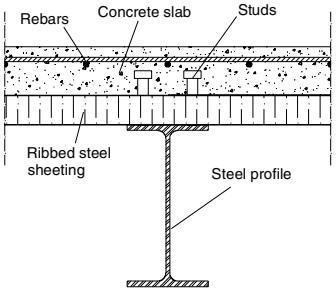

Figure 1. Steel-concrete composite beam.

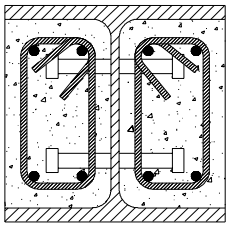

Figure 2. The composite column

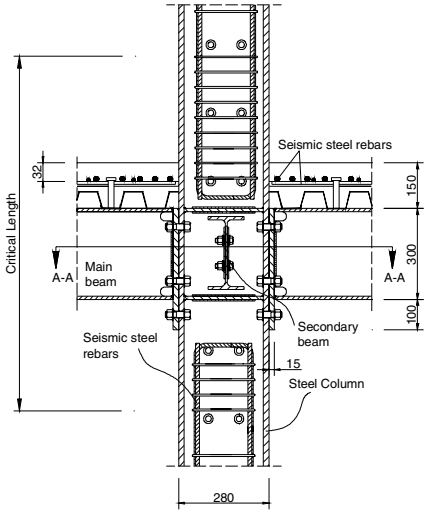

Figure 3. Lateral view (B-B cross section) of the interior joint

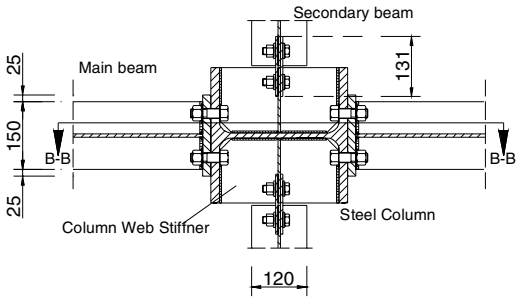

Figure 4. Plan view (A-A cross section) of the interior joint

Table 1. Joint details

	Internal joint	External joint
Beam	IPE 300	IPE 300
Column	HEB 280	HEB 260
Slab thickness	150 mm	150 mm
End-plate thickness	15 mm	15 mm
Sheeting	Brollo EGB 210	Brollo EGB 210
Bolts	M24 10.9	M24 10.9
Steel mesh	ϕ 6 @ 150 mm	ϕ 6 @ 150 mm
Longitudinal additional rebars	4 ϕ 12 (2 for each side)	4 ϕ 12 (2 for each side)
Transverse additional rebars	6 ϕ 12 for each side	5 ϕ 12 for beam side 2 ϕ 12 for the extended side

MAIN EXPERIMENTAL RESULTS

Full-scale substructures representing the interior joint in Fig. 5 have been subjected to monotonic and cyclic tests at the Laboratory for Materials and Structures Testing of the University of Pisa [2]. Both tests were carried out under controlled displacements according to the schemes presented in Fig. 6. The monotonic test permitted to determine the ultimate resistance and rotational capacity of the joints, while cyclic tests allowed their dissipative capacities and ductility to be evaluated, as well as the reduction of stiffness and resistance. The joint behaviour of substructures was summarized by means of moment-rotation relationships. In detail, the joint rotation on the right-hand side reads: $\varphi_r = \varphi_{br} - \varphi_f$, where φ_{br} represents the rotation of the beam at the end plate level and φ_f denotes the rotation of the column. In addition to the joint rotation φ_r, the measuring apparatus allowed the following rotations to be estimated: $\varphi_{conn,r} = \varphi_r - \varphi_c$ and $\gamma_{sp} = \varphi_c - \varphi_f$, where the connection rotation $\varphi_{conn,r}$ and the shear deformation γ_{sp} of the column web panel, respectively, as showed in Fig. 7, and φ_c defines the column rotation in the panel zone. Analogous definitions hold for the joint and the connection on the left-hand side.

The panel shear $V_{wp.Ed.eff}$ depends on the lever arms z_{eq} [8] [9] and therefore, assumptions representative of observed experimental behaviour must be made, which is done following in part the approach proposed in [12]. For the negative moment $M^-_{Rd.conn}$, the resulting upper force is assumed to be located at the level of the longitudinal reinforcing bars. For the positive moment $M^+_{Rd.conn}$, the resulting force is assumed to be located at the mid height of the concrete slab, which defines z_{eq}^-. The level arm z_{eq} then becomes equal to $0.5(z_{eq}^+ + z_{eq}^-)$, which reads 402 mm.

Overall joint behaviour

The moment-rotation and shear-panel distortion relations of an internal joint are illustrated in Fig. 19. The inelastic response concentrated in the end plate and the column flanges, as well as in shear in the column web panel, allowing for plastic joint rotations of over 35 mrad, as required by Eurocode 8 [7].

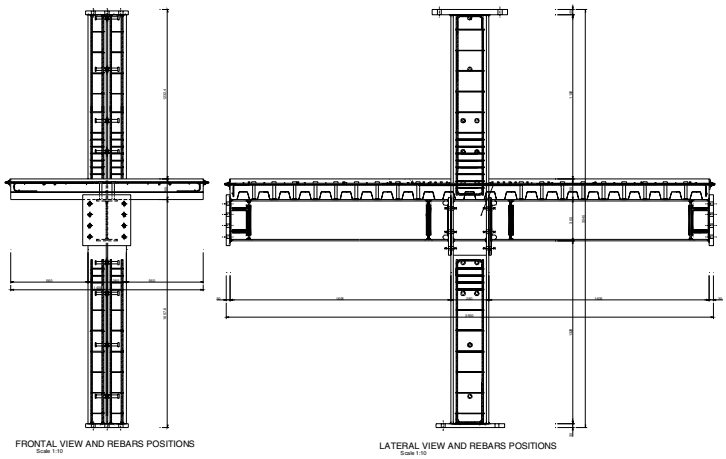

Figure 5. Substructure of an interior joint tested at the University of Pisa

The joint exhibited very high ductility, showing well balanced exploitation of the inelastic resources of both the column web panel in shear and the connection, as shown in Figs. 9a and 9b, respectively. In this case, strut and tie mechanisms in the concrete, as provided for by EC8 [7], were not fully activated. In fact, failure of Mechanism 1 occurred at about 14 mrad (see Figs. 8b and 10a), which caused overloading of Mechanism 2, with consequent sliding of the column with respect to the concrete slab (see Fig. 10b).

Under cyclic loading, the applied force vs. interstorey drift hysteresis in Fig. 11 confirms the favourable behaviour of the internal joint sub-structure, which could achieve interstorey drift levels of about 5 per cent without any significant reduction of strength or stiffness.

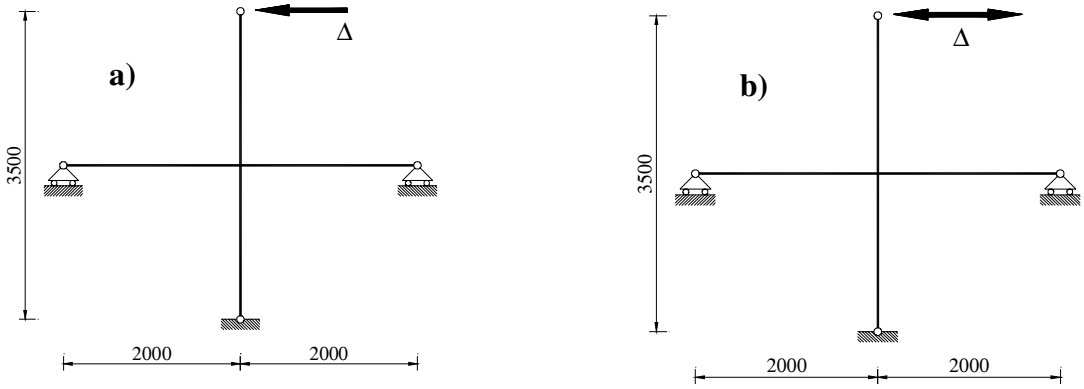

Figure 6. Test on an interior joint: a) quasi-static monotonic loading; b) quasi-static cyclic loading.

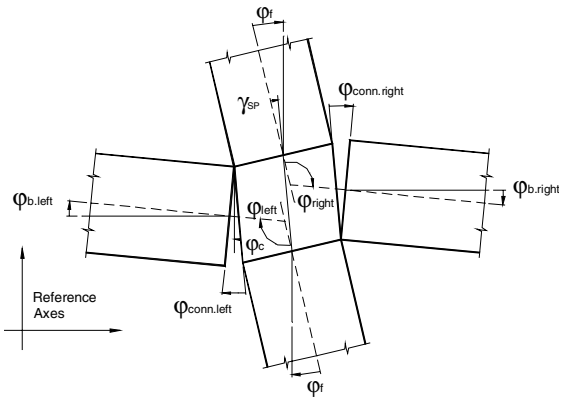

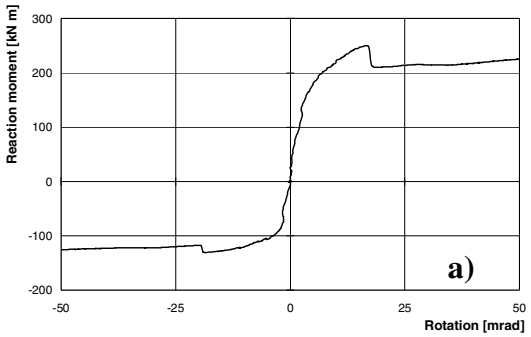

Figure 7. Definition of rotations for an interior joint.

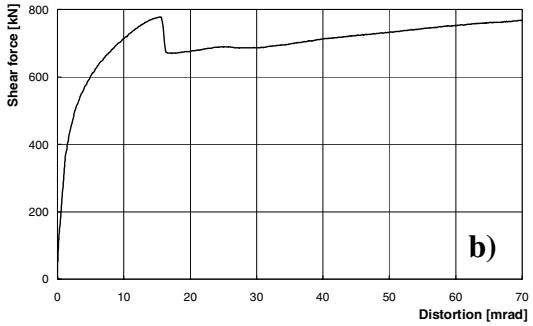

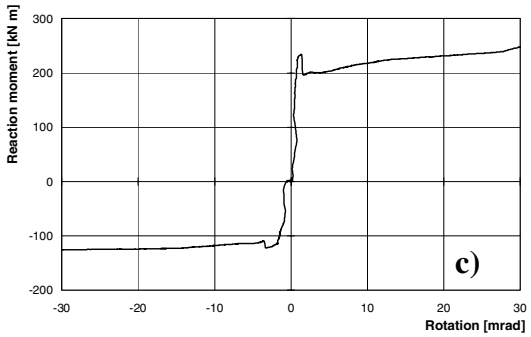

Figure 8. Monotonic response of an interior joint: a) moment vs. joint rotation; b) shear force vs. panel rotation; c) moment vs. connection rotation

Evaluation of internal forces

In order to determine the internal forces acting on the composite beam in the two sections shown in Fig. 12 and better interpret the joint response, the most significant parameters of the absolute displacement were experimentally measured, as well as the forces and reactions applied to the structure and the deformations of the steel beams and reinforcing bars [2]. The location of the instrumented sections was purposely selected because they were subjected to high bending moments while being sufficiently distant from the joint section to allow us to reasonably assume planarity of the sections. The measurements permitted to evaluate the overall bending moments acting on the sections for the monotonic test, as well as

the forces acting on the slab and the steel profile according to the break-down in Fig. 13, in which the distance of the longitudinal bars from the extrados, C_{SR}, is 80 mm and the location of the normal force in the slab is situated at its centroid, at 47.5 mm from the extrados (see Fig. 14).

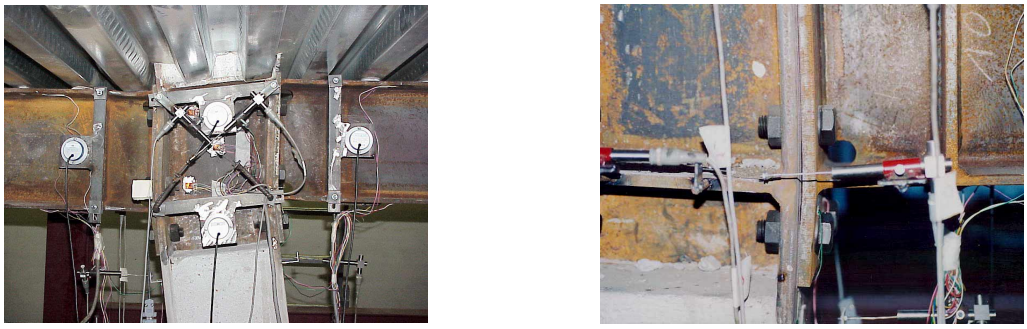

Figure 9. Monotonic test on an interior joint: a) column web distortion; b) connection deformation.

Figure 10. Monotonic test on an interior joint: a) concrete slab crushing; b) column sliding with respect to the concrete slab.

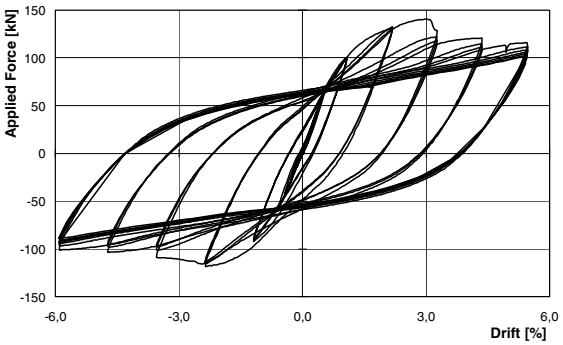

Figure 11. Cyclic test on an interior joint: hysteretic loops of the applied force vs. interstorey drift.

In detail, the measured external reactions were used to determine the overall positive and bending moment, M^{+}_{C} and M^{-}_{C}, acting on the two instrumented sections, while the strain gauges readings yielded the normal force, N_{ST}, and the bending moment, M_{ST}, acting on the steel profile and the normal force N_{SR} acting in the longitudinal reinforcing bars. From horizontal and rotational equilibrium, the axial force and the bending moment acting in the concrete slab, N_{CS} and M_{CS}, could be deducted for both positive and negative moment conditions:

$$N^{+}_{CS} + N^{+}_{ST} + N^{+}_{SR} = 0 \qquad \textbf{(1.a)}$$

$$M^{+}_{C} + M^{+}_{ST} + M^{+}_{CS} + \left(N^{+}_{CS} + N^{+}_{SR}\right) \cdot \left(\frac{h_b}{2} + h_{rss} + \frac{h_{cls}}{2}\right) + N^{+}_{SR} \cdot c_{SR} = 0\,, \qquad \textbf{(1.b)}$$

$$N_{CS}^{-} + N_{ST}^{-} + N_{SR}^{-} = 0 \text{ e} \quad \textbf{(2.a)}$$

$$M_{C}^{-} + M_{ST}^{-} + M_{CS}^{-} + \left(N_{CS}^{-} + N_{SR}^{-}\right) \cdot \left(\frac{h_b}{2} + h_{rss} + \frac{h_{cls}}{2}\right) + N_{SR}^{-} \cdot c_{SR} = 0 \quad \textbf{(2.b)}$$

where h_b is the height of the steel beam, h_{rss} is the height of the ribbed sheeting, h_{cls} is the thickness of the concrete layer above the sheeting collaborating with the steel profile, and c_{SR} is the height of the centroid. The apices + or - indicate whether the internal force refers to the section subjected to positive or negative bending moment.

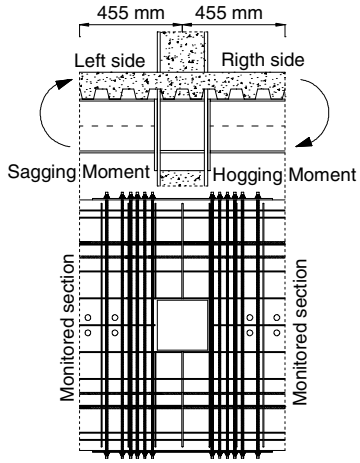

Figure 12. Instrumented sections of a composite beam.

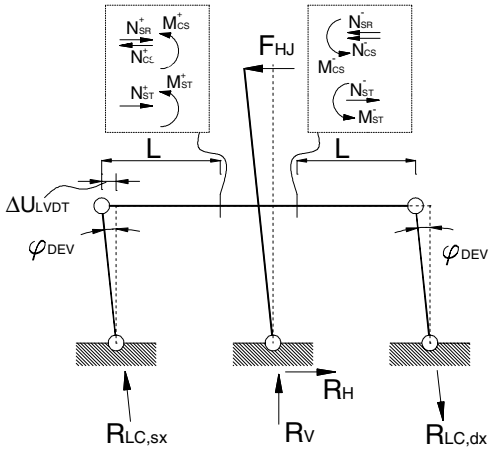

Figure 13. Structural scheme for calculation of internal forces.

In calculating the axial force acting on the slab subjected to tension, the concrete contribution, N^{-}_{CS}, has been included by using a decreasing exponential tension-stiffening model [14]. Figures 16 and 17 show the variation of the normal force and bending moment acting on the monitored section subjected to negative bending moment. As can be seen from Fig. 16, the contribution of tension-stiffening consequent to the progressive cracking of the slab (see Fig. 18) decreases, until it vanishes for drift over about 7%. In the equilibrium calculations for positive moments, the tensile force acting in the longitudinal bars, N^{+}_{SR}, has been considered, thus accounting for interaction effects in the joint (see Fig. 19).

Figures 20 and 21 show the variation of the axial force and bending moment acting in the monitored section subjected to positive bending moment. Interaction between the forces acting on each side of the beam-column joint is activated in the slab by the transfer of the tensile force acting on the longitudinal bars, which are anchored in the compressed zone (see Fig. 22). Such phenomenon and, above all, the effect of the large distortions of the column web panel (see Figs. 23 and 24), induce a further increase in the axial force in the concrete, which causes early fracture in the area of contact with the column flange (Figs. 10 and 11), resulting in a sudden decrease in the forces, as can be seen in Figs. 16, 17, 20, and 21.

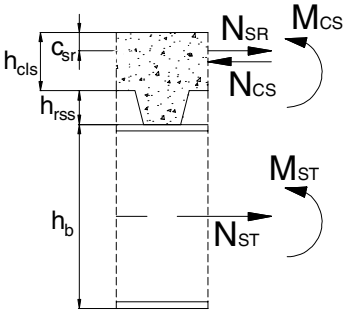

Figure 14. The internal forces acting in the composite section .

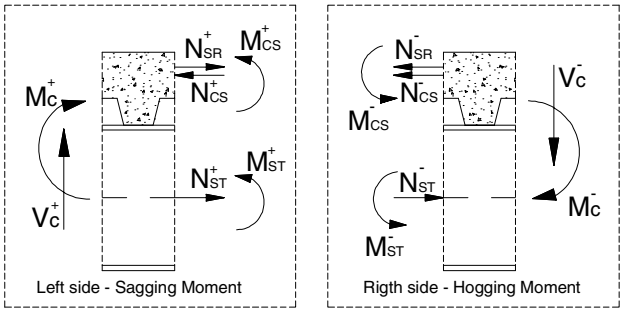

Figure 15. Break-down of the bending moment in the composite beam.

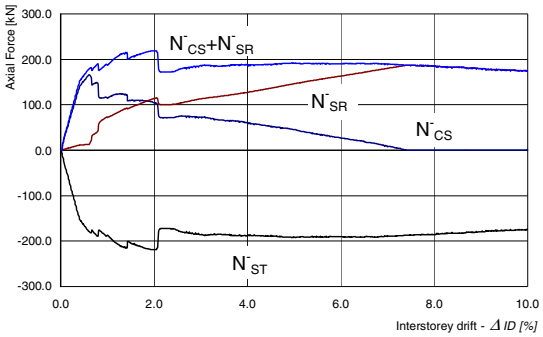

Figure 16. Axial force in the section subjected to hogging moment.

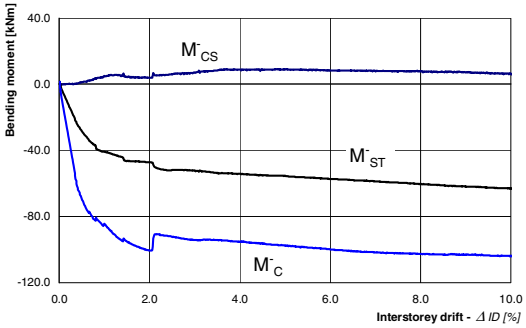

Figure 17. Bending moment in the composite section, subjected to hogging bending moment.

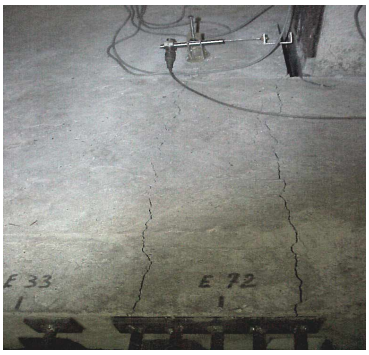

Figure 18. Cracking in the slab under tension.

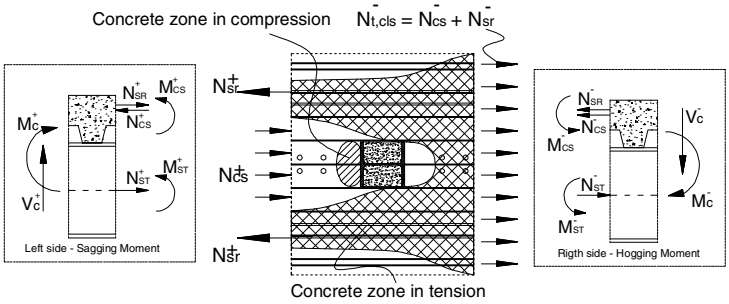

Figure 19. Effect of force interaction in the slab.

MECHANICAL MODELLING OF AN INTERNAL JOINT

A mechanical model was developed based on the "components method" modeling approach to describe the behavior of the beam-column joints. The components active in transferring the bending moment from the beam to the column were identified by observing the behavior of the joint during testing (see Figs. 23 and 24). For sagging bending moment, the following components were considered: (1) the slab under compression, (5) the lower T-stub subjected to tension, and (4) the upper T-stub subjected to compression. For hogging bending moment, the following components were assumed active: (6) the slab under tension, (3) the lower T-stub subjected to compression, and (2) the upper T-stub subjected to tension (see Fig. 25). The column web panel subjected to shear (7) was modeled using a diagonal spring within an articulated quadrilateral formed by rigid elements. Only the panel area free of concrete was considered to deform in shear, while the immediately overlying portion was assumed infinitely stiff, as confirmed by experimental measurements.

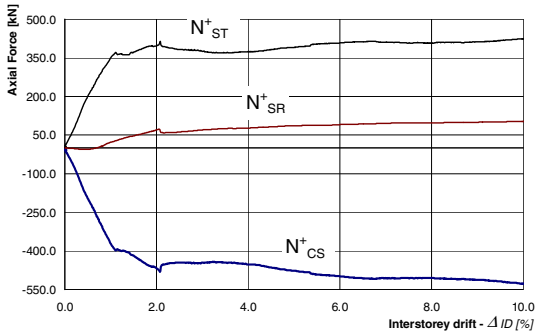

Figure 20. Axial force in the section subjected to sagging moment.

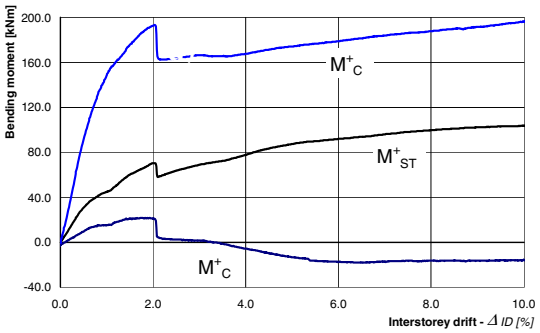

Figure 21. Bending moment in the composite section subjected to sagging moment.

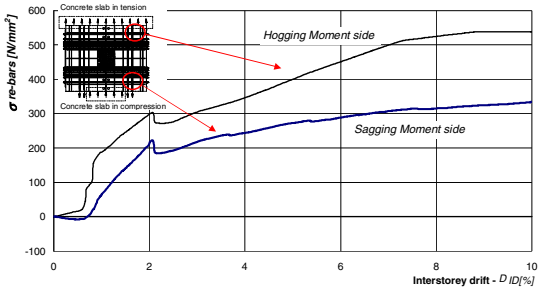

Figure 22. Tensile stress in a reinforcement bar in the monitored sections.

Figure 23. Column web distortion in an internal joint during monotonic test.

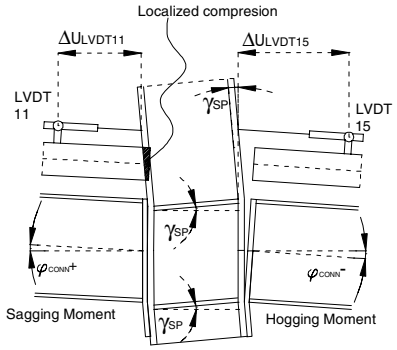

Figure 24. Schematic representation of deformation of the internal joint.

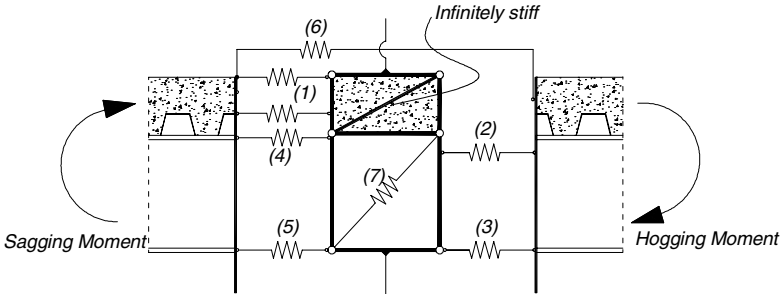

Figure 25. Mechanical model refined on the basis of the results of monotonic tests.

The known internal forces in the connections include the shear, $V_{C,conn}$, and the bending moments on the left and right hand sides of the substructure (see Fig. 13):

$$M^{+}_{C,conn} = R_{LC,sx} \cdot \cos(\varphi_{DEV}) \cdot L_{conn} \;;\; M^{-}_{C,conn} = R_{LC,dx} \cdot \cos(\varphi_{DEV}) \cdot L_{conn} \qquad \textbf{(3)}$$

where L_{conn} is the distance between the lateral restraints and the connection (see Fig. 26). The axial force and the bending moment acting respectively in the steel profile, $N_{ST,conn}$ and $M_{ST,conn}$, and in the slab, $N_{CS,conn}$ and $M_{CS,conn}$, are unknown (see Fig. 27). They were derived on the basis of equilibrium considerations. Based on a suitable kinematic model by which it is assumed that the beam and slab have the same curvature, the axial force acting on the steel beam, $N_{ST,conn,}$ can be calculated by imposing internal equilibrium on the composite beam (see Fig. 28) [15]. This permits to pose the following differential equation:

$$\frac{d^2 N_{ST}(x)}{dx^2} - \alpha^2 \cdot N_{ST}(x) = \beta \cdot M_C(x) \qquad \textbf{(4)}$$

where, for the case at hand, constants α and β (whose general expressions are reported in [15]) take on the values: $\alpha = 0.033$ and $\beta = 3.013 \times 10^{-6}$, (sagging moment), and $\alpha = 0.0203$ and $\beta = 5.914 \times 10^{-7}$ (hogging moment) . Equation (4) must satisfy the associated boundary conditions $N(x=0) = 0$ and $N(x=L) = N_{ST}$, alternatively assigning N_{ST} the values of N^{+}_{ST} and N^{-}_{ST} at the monitored sections (see Fig. 26).

Adopting the reasonable hypothesis that the shear V_C is transmitted to the column solely by the steel connection, the equilibrium of the steel beam between the monitored section and the connection can be expressed by (see Fig. 29):

$$M_{ST,conn} - M_{ST} - V_C \cdot \Delta L + \Delta F \cdot \frac{h_b}{2} = 0 \qquad \textbf{(5)}$$

, allowing to obtain the bending moment, $M_{ST,conn}$, acting in correspondence to the beam-column joints. Lastly, by imposing equilibrium on the rotation and translation of the whole composite beam in

correspondence to the connection, one can obtain for the joint subjected respectively to hogging and sagging moments:

$$M^{-}_{C,conn} - M^{-}_{ST,conn} - M^{-}_{CS,conn} - N^{-}_{ST;conn} \cdot \frac{h_b}{2} - N^{-}_{CS,conn} \cdot \left(h_{rss} + \frac{h_{cls}}{2} \right) = 0 \quad \textbf{(6.a)}$$

$$N^{-}_{ST,conn} - N^{-}_{CS,conn} = 0 \quad \textbf{(6.b)}$$

$$M^{+}_{C,conn} - M^{+}_{ST,conn} - M^{+}_{CS,conn} - N^{+}_{ST,conn} \cdot \frac{h_b}{2} - N^{+}_{CS,conn} \cdot \left(h_{rss} + \frac{h_{cls}}{2} \right) + N^{-}_{CS,conn} \cdot \left(h_{rss} + h_{cls} - c_{SR} \right) = 0 \quad \textbf{(7.a)}$$

$$N^{+}_{ST,conn} - N^{+}_{CS,conn} + N^{-}_{CS,conn} = 0 \quad \textbf{(7.b)}$$

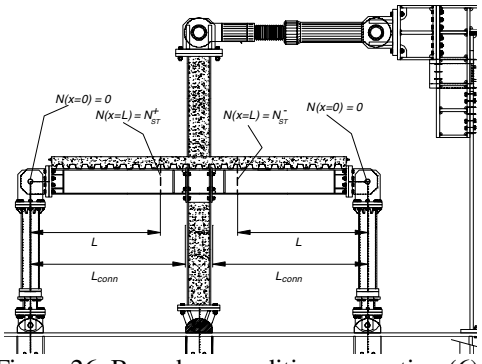

Figure 26. Boundary conditions, equation (6).

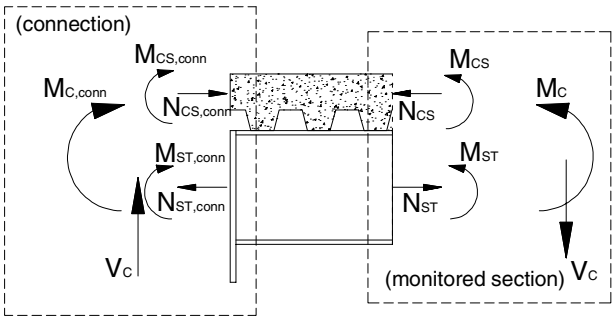

Figure 27. Unknown forces in the connection.

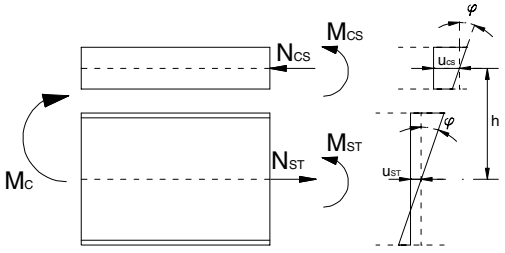

Figure 28. Equilibrium and kinematic model of the composite section [17]

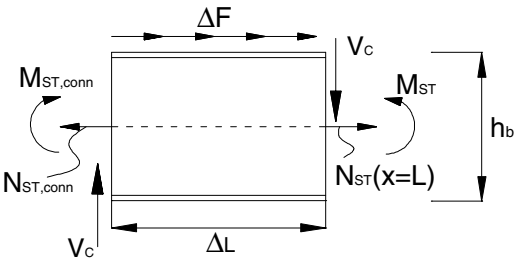

Figure 29. Equilibrium of the steel beam portion between the monitored section and the connection.

From these expressions, it is possible to evaluate the axial forces, $N^{+}_{CS,conn}$ and $N^{-}_{CS,conn,}$ as well as the bending moments, $M^{+}_{CS,conn}$ and $M^{-}_{CS,conn}$, in the slab. Using these internal forces, it is possible to calculate the forces transmitted by the components of the beam-column joints. For the joint subjected to hogging moments, the translational and rotational equilibrium equations become:

$$N^{-}_{CS,conn} - N^{-}_{T-stub,bottom} + N^{-}_{T-stub,top} = 0 \quad \textbf{(8.a)}$$

$$M^{-}_{C,conn} - N^{-}_{T-stub,bottom} \cdot h_1 - N^{-}_{CS,conn} \cdot h_2 = 0 \quad \textbf{(8.b)}$$

, where $N^{-}_{T\text{-}stub,bottom}$ and $N^{-}_{T\text{-}stub,top}$ are respectively the forces acting in the lower and upper T-stub components (see Fig. 30), $N^{-}_{CS,conn}$ is the tensile force in the slab, h_1 is the distance between the two T-stubs, and h_2 defines the position in the slab of the resultant with respect to the upper T-stub. For the joint subjected to sagging moment the equilibrium equations are:

$$N^{-}_{CS,conn} - N^{+}_{T-stub,bottom} + N^{+}_{T-stub,top} - N^{+}_{CS,conn} = 0 \quad \textbf{(9.a)}$$

$$M^{+}_{C,conn} - M^{+}_{CS,conn} - N^{+}_{T-stub,bottom} \cdot h_1 - N^{+}_{CS,conn} \cdot h_2 + N^{-}_{CS,conn} \cdot h_3 = 0 \quad \textbf{(9.b)}$$

in which $N^{+}_{T\text{-}stub,bottom}$ and $N^{+}_{T\text{-}stub,top}$ are the forces acting respectively in the lower and upper T-stubs (see Fig. 31), $N^{+}_{CS,conn}$ is the force of compression in the slab, $N^{-}_{CS,conn}$ is the tensile force transferred by the longitudinal bars of the beam subjected to hogging moments in the compressed zone, and $M^{+}_{CS,conn}$ is the bending moment in the slab. The heights h_1 and h_2 respectively represent the distance between the two T-stubs and the position of the slab centroid, while h_3 is the point of application of $N^{-}_{CS,conn}$ at the centroid of the longitudinal reinforcement.

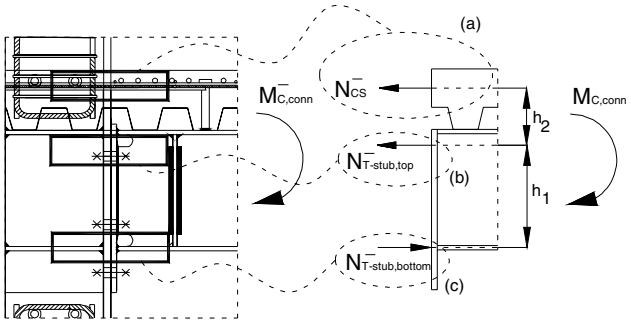

Figure 30. Equilibrium between hogging bending moment and forces in the active components.

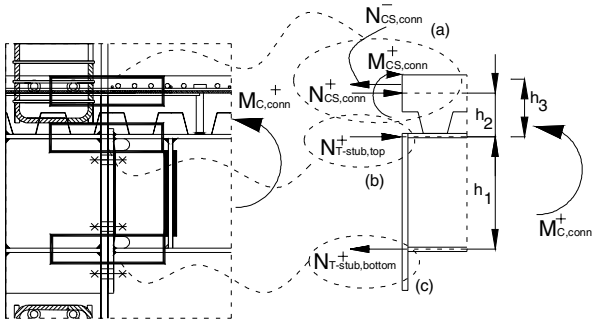

Figure 31. Equilibrium between sagging bending moment and forces in the active components.

From the forces acting in the components of the beam-column joints, the overall shear acting in the panel, V_{WP}, is derived exploiting the horizontal translation equilibrium equation (see Fig. 32):

$$V_{WP} = N^{+}_{CS} + N^{+}_{T-stub,top} + N^{-}_{T-stub,top} - H \qquad \textbf{(10)}$$

in which H is the force applied by the actuator at the top of the column (shear in the composite column). Based on these results, it is possible to describe the pattern of internal forces for the components active in the joint subjected to hogging (see Fig. 33) and sagging bending moments (see Fig. 34), as well as the shear force pattern in the web panel of the column (see Fig. 35).

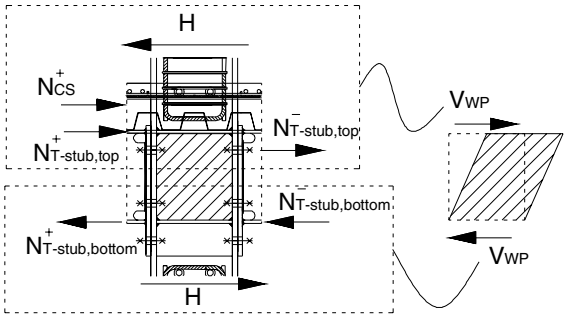

Figure 32. Forces acting on the column web panel.

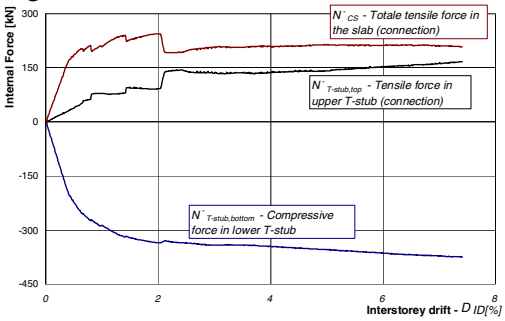

Figure 33. Internal forces in the joint subjected to hogging bending moment.

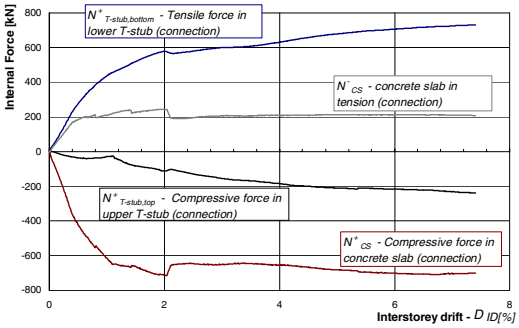

Figure 34. The internal forces in the joint subjected to sagging bending moment.

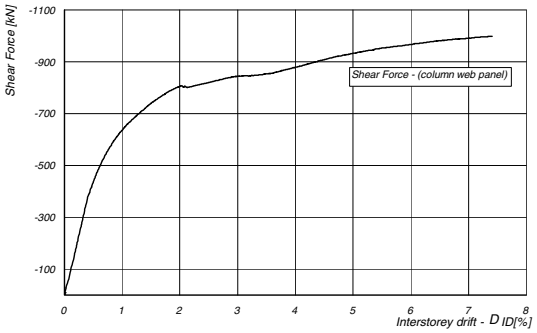

Figure 35. Web panel shear force.

It is also possible to analyze the position of the resultant of the tensile forces in the slab transmitted by the

concrete under tension and the reinforcing bars for the joint section subjected to hogging bending moments (see Fig. 36), as well as the position of the axial force transmitted via the Type 1 mechanism in the joint section subjected to sagging bending moments (see Fig. 37). The results obtained enable making an immediate interpretation of the overall response of the joint.

In the joint subjected to hogging bending moments, the slab tension, $N^{-}_{CS,conn}$, undergoes a sudden fall upon fracture of the concrete under compression (see Fig. 33), at a interstorey drift of about 2%, due to loss of functionality of the type 1 mechanism. The Type 2 mechanism is never activated on the opposite side of the joint. Such a decrease is compensated for in the overall equilibrium of the joint by the force transmitted by the upper T-stub. At the same time, the position of the resultant of the tension force in the slab migrates, as cracking phenomena progresses, towards the position of the reinforcing bars. That force undergoes an abrupt variation (see Fig. 36) which, together with the decrease in the force $N^{-}_{CS,conn}$, provokes a drop in the bending moment transmitted by the joint (see Fig. 8c). For sagging moments, a greater reduction in the moment transferred (see Fig. 8c) occurs due to the lowering of the center of the compression force in the slab in contact with the column (see Fig. 37). Such a change in position is caused by fracture of the upper concrete layers, where compression stresses are higher (see Fig. 19). The compression force in the slab, $N^{+}_{CS,conn}$, undergoes in fact only a small reduction. In the stages subsequent to fracture, it remains nearly unchanged (see Fig. 34), because as the test progresses, the inner, still intact, layers of efficient concrete come to be involved.

Experimental laws governing joint components

The experimental force-displacement laws defining the behavior of components of the mechanical model (see Fig. 25) were determined by coupling the internal forces obtained beforehand with the readings obtained by the transducers in the joints (see Fig. 9b), the web panel (see Fig. 9a), and the slab (see Figs. 10a and 10b). In particular, the force-displacement for the slab in tension (see Fig. 38) was evaluated taking into account the relative displacements occurring in the slab on the two sides of the column, from the transducers shown in Fig. 10. In order to obtain the force-displacement relation for the pair of springs schematizing the slab (see Fig. 39), the bending moment and the compression force acting in the slab were first determined, from which the forces acting in the springs, $N^{+}_{CS,inf}$ and $N^{+}_{CS,sup}$ (see Figs. 40 and 41) could be derived for the mechanical model (see Fig. 25).

The displacement field for the concrete in contact with the column was characterized on the basis of the kinematics observed during testing (see Fig. 42) with the formula:

$$U(s) = \Delta U_{LVDT} - \gamma_{SP} \cdot s + \varphi_{conn}^{+} \cdot \left(s + \frac{h_b}{2} \right) \qquad \textbf{(11)}$$

in which γ_{SP} is the angular distortion of the web panel, φ_{conn}^{+} the rotation of the joint, U_{LVDT} is the displacement revealed by the displacement transducer and h_b is the height of the steel beam; the displacement in correspondence to the upper spring is therefore equal to $U(s = h_{cls}+h_{rss})$, while that in the lower spring is $U(s = h_{rss})$, where h_{rss} and h_{cls} are defined in Fig. 14.

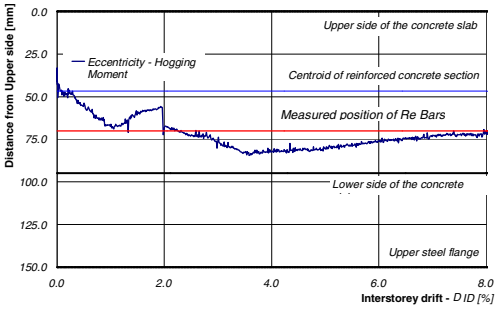

Figure 36. Application level of the tensile force in the slab; connection subjected to hogging bending moments.

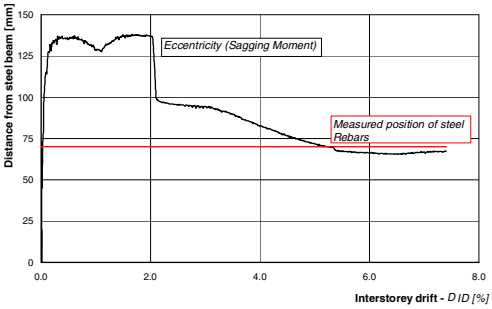

Figure 37. Application level of the compression in the slab; connection subjected to sagging bending moments.

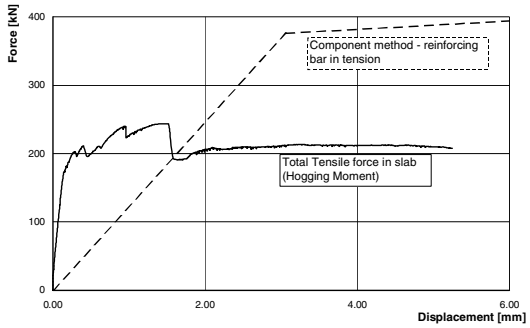

Figure 38. Force- slab displacement law; section subjected to hogging moment

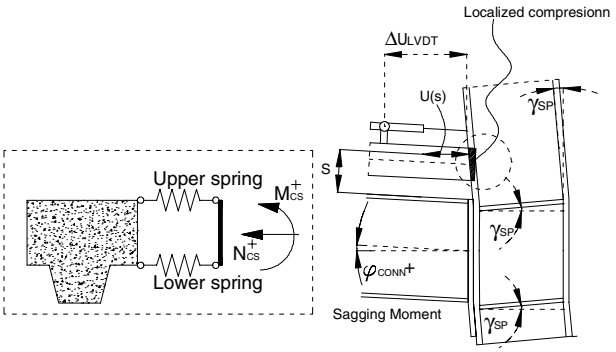

Figure 39. Scheme of the internal forces in the compressed slab

The angle of distortion defining the experimental law for the web panel (see Fig. 42) is obtained from the transducers arranged on the steel column (see Fig. 9a) by the formula:

$$\gamma_{SP} = \mathrm{tg}^{-1}\left[\sqrt{\left(h_{SP}\right)^2 + \left(b_{sp}\right)^2}\,\frac{\left(\Delta U_{LVDT-I} + \Delta U_{LVDT-II}\right)}{2\left(h_{SP} + b_{sp}\right)}\right] \qquad \textbf{(12)}$$

in which ΔU_{LVDT-I} and $\Delta U_{LVDT-II}$ are the absolute value displacements recorded by the transducers and h_{SP} and b_{SP} indicate the height and width of the steel panel. Figures 43-46 represent the force-displacement relationships for the lower T-stub in compression and the upper T-stub in tension in the connection subjected to hogging moment, as well as for the upper T-stub in compression and the lower T-stub in tension in the connection subjected to sagging moments.

Comparison with existing component models

In this subsection, experimental force-displacement relationships are compared with analytical predictions provided by EC4 [6]. Figure 38 illustrates the composite slab subjected to tension and it can be observed that concrete in tension contributes significantly with regard to both stiffness and strength. Clearly, the concrete softening and the indirect effect of concrete crushing is evident in the inelastic range. The disagreement in strength between the experiment and the prediction is due to the fact that yielding of the reinforcing steel is assumed in EC4 while this limit state did not happen during testing. Shear distortion of the column web panel is illustrated in Fig. 42. Fairly good agreement is obtained with the prediction by the Krawinkler's model [12,13] which slightly underestimates the hardening behavior of the web panel. Conversely, in the model suggested by EC3 [3], the lever arm z_{eq} described earlier, only captures the global stiffness and strength properties of the panel behavior. The last comparison deals with the bottom T-stub subjected to tensile forces. Its non-linear behavior is tracked quite well by the simple bilinear model suggested by EC3 [3]. The strain-hardening part of the prediction derives from experimental data collected by Bursi et al. [16].

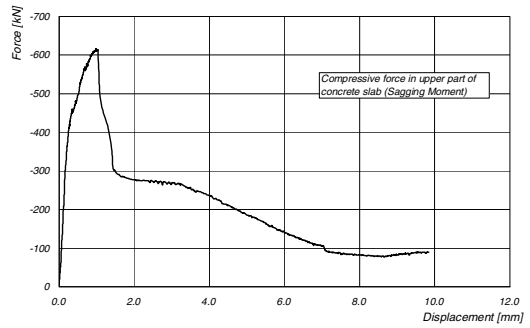

Figure 40. Force-displacement law for the upper spring of the slab scheme.

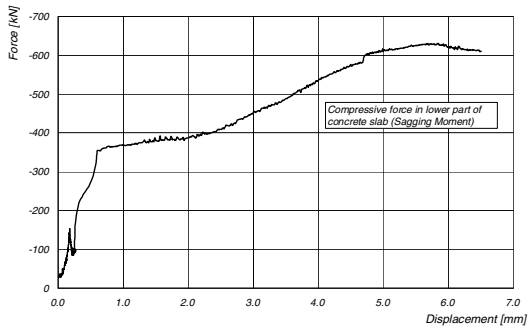

Figure 41. Force-displacement law for the lower spring of the slab scheme.

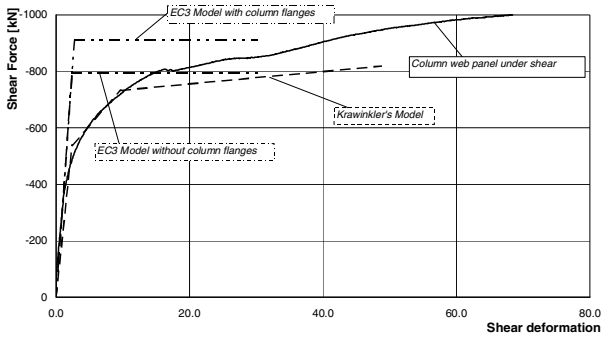

Figure 42. Shear force acting on the web panel as a function of the distortion.

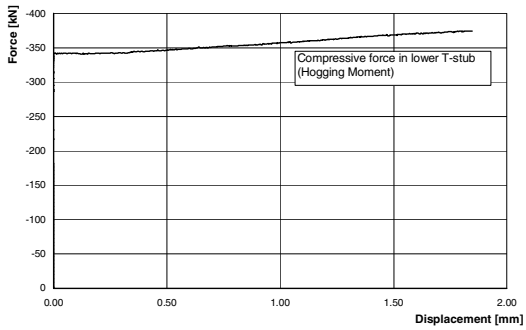

Figure 43. Force-displacement law for the compressed lower T-stub; joint section subjected to hogging bending moment.

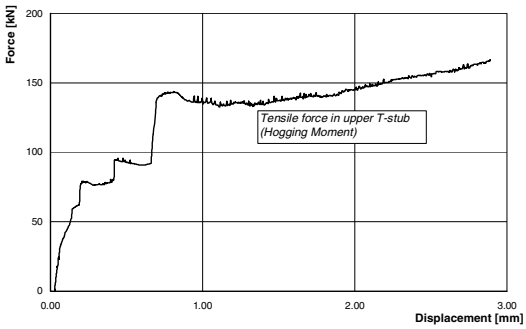

Figure 44. Force-displacement law for the upper T-stub under tension; joint section subjected to hogging bending moment.

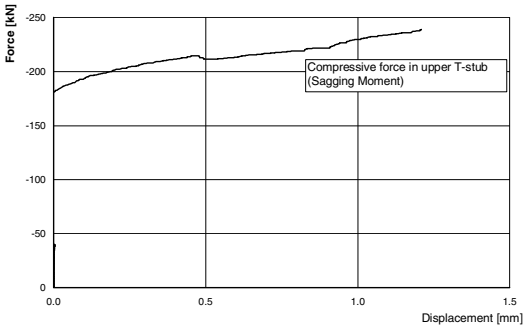

Figure 45. Force-displacement law for the compressed upper T-stub; joint section subjected to sagging bending moment.

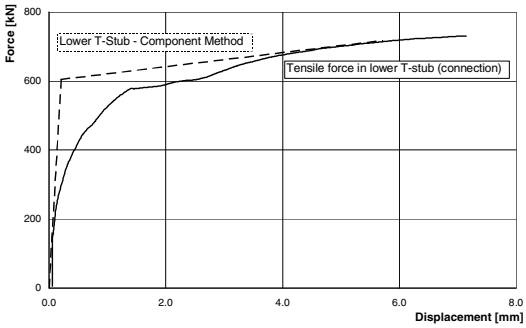

Figure 46. Force-displacement law for the lower T-stub under tension; joint section subjected to sagging bending moment.

CONCLUDING REMARKS

A new mechanical model of an interior partial strength beam-to-column joint used in high ductile steel-concrete composite moment-resisting frame structures has been described. The model which still relies on experimental data is capable of simulating the behavior of steel-concrete composite partial strength joints subjected to monotonic loading. In detail, the model is capable of defining yielding and failure evolution of different components. The component models of the slab have indicated clearly that the compressive strut strength of the composite slab bearing on the column flange depends on the shear stiffness of the column web panel. Moreover, the activation of diagonal compressive struts on column sides induced by transversal reinforcing bars is hindered by the direct bearing of the compressive strut. Some force-displacement relationships provided by the proposed mechanical model have been compared with analytical formulae and current European standards.

ACKNOWLEDGEMENTS

The results presented in this work were obtained in the framework of two European research projects, viz. the ECOLEADER HPR-CT-1999-00059 and the ECSC 7210-PR-250 project, for which the authors are grateful. However, opinions expressed in this paper are those of the writers and do not necessarily reflect those of the sponsors.

REFERENCES

1. Braconi A, Caramelli S, Cioni P, Salvatore W. "Earthquake-resistant composite steel-concrete frames: some constructional considerations". Proceedings of the International Conference on Metal Structures, ICMS 2003. University of Miskolc, Hungary, 2003.
2. Caramelli S., Salvatore W. et al., "Applicability of Composite Structure to Sway Frames, ECSC Project n. 7210-PR-250, Eur Report, European Community, 2004.University of Pisa et al.
3. Bursi O.S., Caramelli S., Fabbrocino G., Molina J., Salvatore W., Taucer F., "3-D Full-scale Seismic Testing of a Steel-concrete Composite Building at Elsa", Contr. No: HPR-CT-1999-00059, Eur Report, European Community, 2004.
4. Bursi OS, Caramelli S, Fabbrocino G, Pinto AV, Salvatore W, Taucer F, Tremblay R, Zandonini R. "Pseudo-dynamic testing of a 3D full-scale high ductile steel-concrete composite MR frame structure at ELSA". Proceedings of the 13th World Conference on Earthquake Engineering. Vancouver, B.C., Canada, Paper no. 507, 2004.
5. prEN 1993-1-8. "Eurocode 3: Design of steel structures. Part 1-8: Design of joints". CEN, European Committee for Standardization. Brussels, Belgium, 2001.
6. prEN 1994-1. "Eurocode 4: Design of composite steel and concrete structures. Part 1: General rules for buildings". CEN, European Committee for Standardization, 2001.
7. prEN 1998-1. "Eurocode 8: Design of structures for earthquake resistance. Part 1: General rules, seismic actions and rules for buildings". CEN, European Committee for Standardization. Brussels, Belgium, 2002.
8. American Institute of Steel Construction, "Seismic provisions for structural steel buildings", AISC 341-02, AISC, Chicago, 2002.
9. Rassati GA, Leon RT, Noè S. "Component modelling of partially restrained composite joints under cyclic and dynamic loading", Journal of Structural Engineering, 2004;130, 2(1): 343-351.
10. Braconi A, Bursi OS, Ferrario F, Salvatore W. "Seismic design of beam-to-column connections for steel-concrete composite moment resisting frames". Proceedings of the Fourth International Conference STESSA 2003: Behaviour of Steel Structures in Seismic Areas. Naples, Italy, 2003, 253-260.
11. Lee S.-J. and Lu L.-W., "Cyclic Tests of Full-scale Composite Joint Subassemblages", Journal of Structural Engineering, ASCE, 1989; (8): 1977-1998.
12. Krawinkler, H, "Shear in beam-column joints in seismic design of steel frames", Engineering Journal, 3rd Quarter, American Institute of Steel Construction, 1978.
13. Krawinkler, H., Bertero, V. V., Popov, E. P., "Inelastic behaviour of steel beam-to-column subassemblages", Technical report EERC 71-7, October, College of engineering University of California, Berkeley, 1971.
14. Stevens, N. J., Uzumeri, S. M., Collins, M. P. and Will, G. T., "Constitutive Model for Reinforced Concrete Finite Element". A.C.I. Structural Journal, vol. 88, n° 1, January-February, 1991.
15. Cosenza, E., Mazzolani, S., "Linear analysis of composite beams with deformable connectors: exact formulas and finite difference solutions", Proceedings of the 1st Italian workshop on composite structures, University of Trento, June, 1993: 1-20 (in Italian).
16. Bursi OS, Ferrario F, Fontanari V, "Non-linear Analysis of the Low-cycle Fracture Behaviour of Isolated Tee Stub Connections" Computers & Structures, 2002, 80:2333-2360.